# Interface phonons of quantum wires

P. A. Knipp and T. L. Reinecke
*Naval Research Laboratory, Washington, D.C. 20375-5000*
(Received 21 October 1991)

We have used the continuum dielectric approach to study the optical-interface-phonon modes of a quantum-wire structure consisting of one material buried within another. Wires with a number of cross-sectional shapes have been studied. Analytical results are presented for wires with elliptical cross sections, of which the circular cross section is a special case. Numerical results using an integral-equation approach are given for wires with arbitrary cross-sectional shapes including rectangles having rounded corners. The dependence of the modes on the wire cross sections and their relation to the vibrational modes of planar quantum wells are discussed. For large wave vectors parallel to the wire or around the wire circumference, the modes are found to approach those of the planar interface. Modes are found to be localized in the corners of the wires or regions of high curvature, and the degree of localization is found to increase with the increasing sharpness of the corners.

## I. INTRODUCTION

Recent advances in growth and microfabrication techniques have made it possible to obtain quasi-one-dimensional wirelike structures of one polar semiconductor material within another. Some of the most interesting work of this kind involves epitaxially grown buried wire structures such as those grown on vicinal surfaces by migration-enhanced molecular-beam epitaxy.[1] In addition, there are a variety of structures which can be produced by etching or lithography techniques. Such methods have produced wires having cross-sectional areas ranging from a few atoms to square micrometers or more. Their cross sections exhibit a variety of shapes, and they have been constructed from a number of semiconductor materials, particularly the III-V's. The semiconductor wire structures are beginning to attract increased attention from both experimental and theoretical points of view. Such research is expected to lead to a better understanding of the effects of confinement and decreased dimensionality on the electronic, optical, and transport properties of semiconductor systems, potentially forming the basis for novel technological applications.

Semiconductor quantum-well systems, which consist of a layer of one material such as GaAs within another material such as $Al_xGa_{1-x}As$, have been studied extensively in recent years. In such systems both the electrons and the phonons have been found to be strongly affected by confinement. The effects of confinement on LO phonons and the resulting modification of the electron-phonon interaction have attracted particular attention.[2] Phonons in these structures have been detected experimentally, especially by Raman scattering.[2,3] In systems such as GaAs/AlAs the LO-phonon dispersions of the two bulk materials do not overlap in frequency, and as a result the phonons are localized strongly in the respective layers. The LO phonons which are confined within each layer are often referred to as "bulk" confined phonons. There are also optical phonons which are localized in the vicinity of the interfaces.[4,5] These interface modes are the analogs of the classical surface phonons and plasmons which have been examined extensively over the years.[6] In the case of semiconductor quantum-well systems, the interface modes have been found to play a dominant role in electron relaxation and electron scattering as the well width becomes small.[7] By analogy to the quantum-well case, one expects the phonons in quantum-wire structures to be affected strongly by confinement, giving rise to both interface modes and confined modes. We expect that interface modes may play an important role in electron-phonon coupling, electron relaxation, and electron scattering.

Phonons in quantum-well systems have been studied theoretically using both lattice-dynamics approaches[8-10] and dielectric continuum approaches.[2,4,8] Continuum approaches play an important role in these studies because they provide analytic results for the phonon eigenfunctions from which the electron-phonon coupling can be obtained conveniently. The continuum approach also provides analytical results for phonon frequencies which are expected to be valid for vibrations with wavelengths considerably longer than the interatomic spacing. To date relatively little work has been done on the phonons of quasi-one-dimensional wire structures. A recent Raman-scattering experiment has detected an interface phonon for an array of GaAs wires.[11] Lattice-dynamical calculations for some particular wire arrays have been made recently.[12,13] Constantinou and Ridley[14] have used a hydrodynamical continuum approach to study phonons in wires of circular cross section. It should be noted that their approach differs from the commonly used dielectric continuum approach. Ruppin and Englman[15] have used the dielectric continuum approach to give results for the interface modes of a cylindrical wire. Stroscio[16] has calculated results for the bulk confined modes of a wire of square cross section based on the continuum model. Stroscio *et al.*[17] also have given results for the interface modes of this system, but their treatment did not properly include the boundary conditions. Here our calculation

 

correctly incorporates the boundary conditions, and we present results that differ qualitatively from those of Ref. 17.

In the present work the interface phonon modes of wires with various cross sections are studied within the continuum approach. Here we use standard electrostatic boundary conditions.[18] This approach to the study of interface modes has been substantiated by lattice-dynamical treatments.[8–10] Analytical results are given here for wires of elliptical cross sections, of which the cylindrical wire is a limiting case. It is pointed out that the interface modes of wires of more general cross section, including the rectangular case, cannot be obtained analytically, even within the continuum approach. An integral-equation method is used here to obtain numerically the interface modes of wires of arbitrary cross section. These results are given for wires with rectangular and related cross sections. A number of interesting features emerge from these results. In the continuum approach it is found that, in general, there are an infinite number of interface modes for each wave vector along the wire for all wire geometries. In the case of wires with rectangularlike shapes some interface modes are found to be localized in the corners. As the corners become sharper, these interface modes become increasingly localized at the corners. The relation of all of these interface modes to those of quantum wells is discussed.

## II. FORMALISM

In the present work the dielectric continuum approach[2] is used to study the interface phonons of wire structures. This approach is described briefly now. We consider a model consisting of a single wire with dielectric function $\epsilon_1(\omega)$ embedded in a second material with dielectric function $\epsilon_2(\omega)$ as shown in Fig. 1. Each dielectric function is frequency dependent and is assumed to be isotropic and independent of $\mathbf{k}$. The wire is taken to extend infinitely in the $z$ direction, and several cross-sectional shapes in the $xy$ plane are considered. Each material is taken to be characterized by dispersionless LO and TO phonons, and the dielectric functions are taken to be[19]

$$\epsilon_i(\omega)=\epsilon_\infty^{(i)}\frac{\omega^2-\omega_{\mathrm{LO},i}^2}{\omega^2-\omega_{\mathrm{TO},i}^2},\quad i=1,2\ . \tag{2.1}$$

There exists no free charge in the system, and thus $\nabla\cdot\mathbf{D}=0$ everywhere, where $\mathbf{D}$ is the displacement field. This gives $\epsilon_i(\omega)\nabla\cdot\mathbf{E}=0$ in each material, where $\mathbf{E}$ is the electric field. The effects of retardation are important only for phonon wavelengths comparable to the infrared wavelength $\sqrt{\epsilon}\omega/c$ (Ref. 20) and will be neglected here.

From Eq. (2.1) it is seen that the condition $\epsilon_i(\omega)=0$ describes a (confined) bulk-LO phonon in material $i$, with frequency $\omega_{\mathrm{LO},i}$, and that $\epsilon_i(\omega)=\infty$ gives a (confined) bulk-TO phonon in material $i$. It is straightforward to show that the condition $\epsilon_1(\omega)=-\epsilon_2(\omega)$ describes an interface phonon at a single planar boundary.[2] Here we are interested in the interface modes. For them $\epsilon_i(\omega)\neq 0$ and the condition $\nabla\cdot\mathbf{D}=0$ gives $\nabla\cdot\mathbf{E}=0$ in each material. Because retardation is ignored, the electric field can be derived from a scalar potential $\Phi$ satisfying $\nabla^2\Phi=0$. From translational invariance along the $z$ direction, the potential can be written $\Phi(x,y,z)=\phi(x,y)\exp(ikz)$ where the reduced potential $\phi(x,y)$ satisfies

$$\nabla^2\phi(x,y)-k^2\phi(x,y)=0\ . \tag{2.2}$$

Then the electric field can be written as

$$\mathbf{E}(x,y,z)=[\bar{\mathbf{E}}(x,y)-ik\hat{\mathbf{z}}\phi(x,y)]\exp(ikz)\ ,$$

where the overbar represents the projection of a three-dimensional vector in a direction perpendicular to the wire. Equation (2.2) is the basic two-dimensional wave equation describing the interface modes in these systems. Associated with it are the standard electrostatic boundary conditions imposed at the interface between the media: continuity of $\phi$, which follows from the continuity of the tangential components of $\mathbf{E}$, and continuity of the normal component of $\bar{D}\equiv\epsilon\bar{E}$.[18] The condition that the phonon amplitude vanishes far from the wire specifies an interface mode.

## III. ELLIPTICAL WIRE

First we consider a wire with elliptical cross section having a major axis $R$ and a minor axis $r$. An example with aspect ratio $R/r=2$ is shown in Fig 1. For the case of an elliptical cross section, Eq. (2.2) and the boundary conditions are separable in elliptical coordinates.[21] These coordinates $(u,v)$ are related to Cartesian coordinates $(x,y)$ by $x=\sqrt{R^2-r^2}\cosh u\cos v$ and $y=\sqrt{R^2-r^2}\sinh u\sin v$. Contours of constant $u$ ($v$) are ellipses (hyperbolas). The foci of these contours are all located at $(x,y)=(\pm\sqrt{R^2-r^2},0)$. The ellipse specified

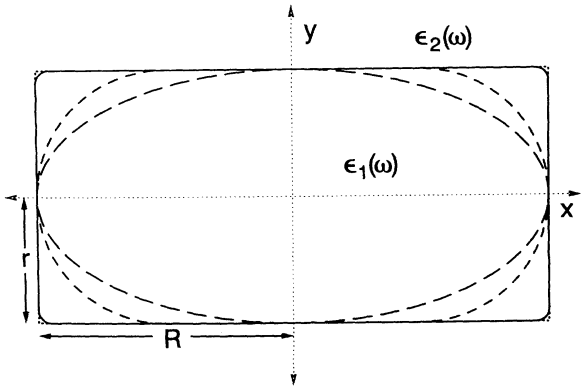


FIG. 1. Drawings of the cross sections of four wires discussed in Secs. III–V. The elliptical cross section discussed in Sec. III is indicated by the long-dashed line. The short-dashed line indicates the example ("oval") studied in Sec. IV. The solid and dotted lines are rectangles with rounded corners and so are approximations to a rectangular wire as discussed in Sec. V. The radius of curvature ($a$) at the corners of the solid line equals $r\times 10^{-1}$, and that of the dotted line is $r\times 10^{-5}$. The notations $r$ and $R$ are shown in the figure.

by $u=u_0\equiv\frac{1}{2}\ln[(R+r)/(R-r)]$ gives the surface of the wire.

Equation (2.2) for $\phi\equiv V(v)U(u)$ is separated in elliptical coordinates yielding an "angular" equation

$$\frac{d^2V}{dv^2}+(\alpha-2q\cos 2v)V=0 \tag{3.1}$$

and a "radial" equation

$$\frac{d^2U}{du^2}-(\alpha-2q\cosh 2u)U=0\ . \tag{3.2}$$

Here the real quantity $\alpha$ represents the separation constant, and $q$ equals $k^2(r^2-R^2)/4<0$. We begin by looking at Eq. (3.1). Because of periodicity around the wire $[V(v+2\pi)=V(v)]$, the quantity $\alpha$ is quantized. For a given $q$ there exist an infinite number of solutions, each of which is specified by a (nonnegative) integer index $m$ which plays the role of an azimuthal quantum number. These solutions fall into four different symmetry classes depending on whether $V(v)$ is symmetric or antisymmetric with respect to reflection through each of the $x$ and $y$ axes. Depending on this symmetry the $m$th eigenvalue $\alpha_m$ of Eq. (3.1) is either $a_m$ or $b_m$, and its corresponding eigenfunction is a periodic Mathieu function, either $\mathrm{ce}_m(v)$ or $\mathrm{se}_m(v)$, respectively.[22,23] All of these quantities are continuous functions of $q$. When the eigenvalue $a_m$ ($b_m$) is inserted into Eq. (3.2), the solution of $U(u)$ is proportional to $\mathrm{Ce}_m(u)$ [$\mathrm{Se}_m(u)$] for $u\le u_0$ and is proportional to $\mathrm{Fek}_m(u)$ [$\mathrm{Gek}_m(u)$] for $u\ge u_0$. Of these four functions (associated Mathieu functions), the former pair are finite near $u=0$ but diverge as $u\to\infty$, and the latter pair diverge as $u\to 0$ but are finite as $u\to\infty$.

$$V_m(v)=\mathrm{ce}_m(v,q)\ ,$$

and (3.3)

$$U_m(u)=\begin{cases}\mathrm{Ce}_m(u,q)\mathrm{Fek}_m(u_0,q) & \text{if } u\le u_0\\ \mathrm{Ce}_m(u_0,q)\mathrm{Fek}_m(u,q) & \text{if } u\ge u_0\ ,\end{cases}$$

where $m$ is a nonnegative integer. If $m$ is even (odd) the solutions are even (odd) in $x$. From Eq. (3.3) it can be seen that $\phi(u,v)$ is everywhere finite and continuous, that $\nabla\Phi$ vanishes far from the wire, and that the only discontinuity in the derivative of $\phi$ occurs at $u=u_0$ in the direction normal to the wire boundary. Continuity in the normal component of $\mathbf{D}=\epsilon(\omega)\mathbf{E}$ across this interface gives

$$\frac{\epsilon_1(\omega_m)}{\epsilon_2(\omega_m)}=\frac{(\partial/\partial u)[\ln \mathrm{Fek}_m(u,q)]|_{u=u_0}}{(\partial/\partial u')[\ln \mathrm{Ce}_m(u',q)]|_{u'=u_0}}\ . \tag{3.4}$$

By substituting Eq. (2.1) into Eq. (3.4), one obtains the dispersion relations for the interface eigenmodes $\omega_m(k)$.

For $V(v)$ odd in $y$

$$V_m(v)=\mathrm{se}_m(v,q)\ ,$$

and

$$U_m(u)=\begin{cases}\mathrm{Se}_m(u,q)\mathrm{Gek}_m(u_0,q) & \text{if } u\le u_0\\ \mathrm{Se}_m(u_0,q)\mathrm{Gek}_m(u,q) & \text{if } u\ge u_0\ ,\end{cases} \tag{3.5}$$

where $m$ is a positive integer. In this case if $m$ is even (odd) the solutions are odd (even) in $x$. The interface-mode dispersion relations are obtained from the continuity of the normal component of $\mathbf{D}$:

$$\frac{\epsilon_1(\omega_m)}{\epsilon_2(\omega_m)}=\frac{(\partial/\partial u)[\ln \mathrm{Gek}_m(u,q)]|_{u=u_0}}{(\partial/\partial u')[\ln \mathrm{Se}_m(u',q)]|_{u'=u_0}}\ . \tag{3.6}$$

At $k=0$ the solutions simplify considerably. If $V(v)$ is even in $y$ then $\alpha_m=m^2$, and $V_m(v)=\cos mv$ where $m$ is a nonnegative integer. The radial part of the solution is then given by

$$U_m(u)=\begin{cases}u_0, & u\le u_0,\ m=0\\ u, & u\ge u_0,\ m=0\\ \exp(-mu_0)\cosh mu, & u\le u_0,\ m>0\\ \exp(-mu)\cosh mu_0, & u\le u_0,\ m>0\end{cases} \tag{3.7}$$

and the dispersion relations are given by

$$\frac{\epsilon_1(\omega_m)}{\epsilon_2(\omega_m)}=\frac{(R-r)^m+(R+r)^m}{(R-r)^m-(R+r)^m}\ . \tag{3.8}$$

For $k=0$ and $V(v)$ odd in $y$, then $\alpha_m=m^2$ and $V_m(v)=\sin mv$ and

$$U_m(u)=\begin{cases}\exp(-mu_0)\sinh mu, & u\le u_0\\ \exp(-mu)\sinh mu_0, & u\ge u_0\ ,\end{cases} \tag{3.9}$$

$$\frac{\epsilon_1(\omega_m)}{\epsilon_2(\omega_m)}=\frac{(R-r)^m-(R+r)^m}{(R-r)^m+(R+r)^m}\ , \tag{3.10}$$

where $m$ is a positive integer.

A wire with a circular cross section is a special case of the elliptical cross section, and the interface phonons have been derived previously for it in Ref. 15 using this same continuum approach. For a circular cross section of radius $r$ the solutions are given simply in circular cylindrical coordinates $[\phi(\rho,\theta)\equiv U(\rho)V(\theta)]$, where $(\rho,\theta)$ are the radial and angular variables, respectively. The angular solutions $V_m(\theta)$ are either $\sin m\theta$ or $\cos m\theta$, and the radial solutions are expressed as Bessel functions of imaginary argument $(K_m, I_m)$

$$U_m(\rho)=\begin{cases}K_m(kr)I_m(k\rho), & \rho<r\\ K_m(k\rho)I_m(kr), & \rho\ge r\ .\end{cases} \tag{3.11}$$

The phonon-dispersion relations $\omega_m(k)$ are given by

$$\frac{\epsilon_1(\omega_m)}{\epsilon_2(\omega_m)}=\frac{(\partial/\partial\rho)[\ln K_m(k\rho)]|_{\rho=r}}{(\partial/\partial\rho')[\ln I_m(k\rho')]|_{\rho'=r}}=-\frac{[K_{m+1}(kr)+K_{m-1}(kr)]I_m(kr)}{[I_{m+1}(kr)+I_{m-1}(kr)]K_m(kr)}\ . \tag{3.12}$$

For all wire cross sections the interface-mode frequencies $\omega_m(k)$ lie in the reststrahlen regions of either one or the other material; i.e., either $\omega_{\mathrm{TO},1}<\omega_m(k)<\omega_{\mathrm{LO},1}$ or

$\omega_{\mathrm{TO},2} < \omega_m(k) < \omega_{\mathrm{LO},2}$. The quantity

$$\lambda_m \equiv \frac{\epsilon_1(\omega_m)+\epsilon_2(\omega_m)}{\epsilon_1(\omega_m)-\epsilon_2(\omega_m)} \tag{3.13}$$

is a convenient way to display the interface-mode dispersion relations $\omega_m(k)$ which is independent of choice of the material parameters $(\epsilon_0, \epsilon_\infty, \omega_{\mathrm{TO},i}, \omega_{\mathrm{LO},i})$. For example, the values for $\lambda_m(k)$ for an elliptical cross section having $R/r=2$ are shown in Fig. 2. The quantity $\lambda_m$ depends only on $k$ and the wire geometry $(R,r)$. In order to convert from $\lambda_m$ to the interface-mode frequencies for particular materials, one substitutes Eq. (2.1) into Eq. (3.13). For instance, $\lambda=1$ corresponds to $\omega$ equaling either $\omega_{\mathrm{TO},1}$ or $\omega_{\mathrm{LO},2}$, whereas $\lambda=-1$ corresponds to $\omega$ equaling either $\omega_{\mathrm{LO},1}$ or $\omega_{\mathrm{TO},2}$. Thus the region $-1<\lambda<1$ corresponds to the two reststrahlen regions, and its endpoints $\lambda=\pm 1$ correspond to the four bulklike modes in the two materials. A useful point to note is that $\lambda=0$ corresponds to $\omega=\omega_{\mathrm{IF},1}$ or $\omega=\omega_{\mathrm{IF},2}$ where $\omega_{\mathrm{IF},1}$ and $\omega_{\mathrm{IF},2}$ are the (dispersionless) interface-mode frequencies of a single planar boundary separating dielectrics 1 and 2, as noted in Sec. II.

A few qualitative aspects of the analytical results for the elliptical and circular cases are worth noting. First we summarize their similarities. When either $k$ or $m$ becomes large the modes localize very strongly to the interface and have nearly vanishing values of $\lambda$ in a manner similar to the case of the interface modes of a flat surface. Examples of this spatial behavior for a wire of circular cross section can be seen in Figs. 3(a) and 3(b) for the potential $\phi(x,y)$ generated by the modes with $(kr,m)$ equaling (5.0,0) and (1.0,8) respectively. The reason for this behavior is that the wavelength becomes so small that the electric field generated by the charge separation is of short range, giving rise to small coupling with other portions of the wire. Because of their localization near the interface, modes for large $k$ and $m$ are expected to couple only weakly with electrons confined to the wire interior. The quantity $\lambda_m$ for the ellipse is shown in Fig. 2 as a function of $kr$, for low values of $m$. Note that $\lambda_m(k)\to 0$ for large $m$ or $k$. A particularly interesting feature involves the low-$k$ behavior of the $m=0$ interface mode. For both the circular and elliptical cases $\lambda_{m=0}(k\to 0)$ approaches unity, which corresponds to $\omega_{m=0}(k\to 0)$ approaching either $\omega_{\mathrm{LO},2}$ or $\omega_{\mathrm{TO},1}$. As $k\to 0$, the reduced potential $\phi$ generated by the $m=0$ mode is constant within the wire, and thus E is parallel to the wire axis in this region. At large radial distances $\rho$ outside the wire, the field $\bar{E}$ varies inversely with $\rho$. In Sec. IV this behavior will be seen to occur for wires of arbitrary cross section.

The solutions for the circular case are qualitatively

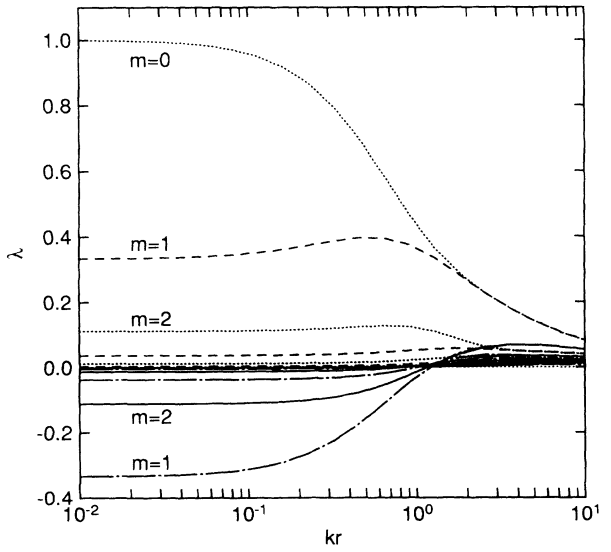


FIG. 2. Dependence of eigenvalues $\lambda_m$ [defined by Eq. (3.13)] as a function of $kr$ for a wire with elliptical cross section where $r$ is the minor axis of the ellipse shown in Fig. 1 and $k$ is the wave vector along the wire. Dotted lines indicate modes that are symmetric in both $x$ and $y$, dot-dashed lines are modes symmetric in $x$ but antisymmetric in $y$, dashed lines are modes antisymmetric in $x$ and symmetric in $y$, and solid lines indicate modes that are antisymmetric in both $x$ and $y$. The lowest mode indices $m$ from Eqs. (3.4) and (3.6) are indicated on each curve.

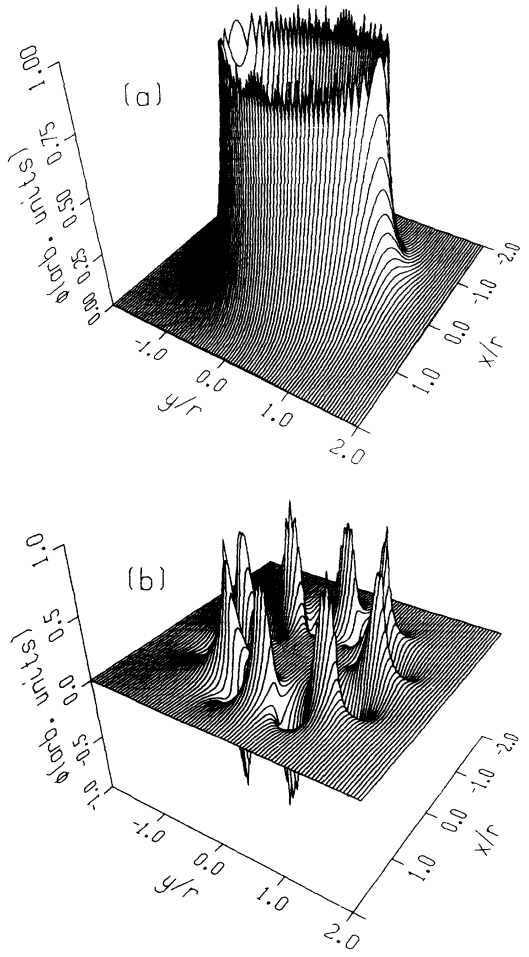


FIG. 3. The reduced potential $\phi(x,y)$ from Eq. (2.2) generated by the interface mode of a wire with circular cross section for (a) $kr=5$ and mode index $m=0$ or (b) $kr=1$ and $m=8$.

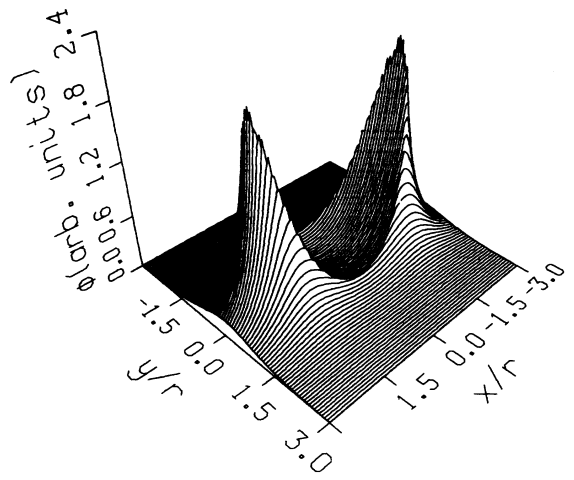


FIG. 4. The reduced potential $\phi(x,y)$ generated by the $m=0$, $kr=2$ interface mode of a wire with elliptical cross section and aspect ratio $R/r=2$.

similar to those of the elliptical case except for a few features. Careful inspection of Eq. (3.12) reveals that for the circular case at $k=0$, only one (the $m=0$) value of $\lambda$ differs from zero. All values of $\lambda_m(k=0)$ are nonzero for an ellipse. Also, for the circular case the two modes with the same value of $m$ are degenerate owing to rotational symmetry. They are not degenerate for the ellipse. Finally, the loss of isotropy allows for the possibility of angular localization. Figure 4 shows that the potential generated by the $m=0$ mode for $kr=2$ is greatly enhanced near the vertices of the ellipse. The cause of this partial localization is seen by inspection of Eq. (3.1). If this equation is interpreted as a Schrödinger equation, then the minimum of the potential energy occurs at $\cos 2v=1$ corresponding to the ellipse vertices. This tendency of interface modes to localize at regions of high curvature along the boundary will be seen to be more pronounced for wires with rectangular cross sections, described in Sec. V.

## IV. INTEGRAL EQUATION

For most wire geometries, including the simple case of a square cross section, Eq. (2.2) and the boundary conditions cannot be separated into two one-dimensional problems. This necessitates the solution of a scalar wave equation with appropriate boundary conditions over an infinite two-dimensional space, which must be done numerically for most geometries. In this section we transform this complicated task into a simpler one, an integral equation over a finite one-dimensional interval. This procedure is commonly used to transform a $d$-dimensional partial differential equation with boundary conditions into a $(d-1)$-dimensional integral equation (see, e.g., Sec. 8.1 of Ref. 21 or Sec. 6.1 of Ref. 24).

Oscillating fields in dielectric systems may be interpreted as being generated by bound charge densities at interfaces. Knowledge of the fields is sufficient to determine the surface charge density $\sigma$ from the boundary condition

$$\bar{E}_{\rm out}-\bar{E}_{\rm in}=4\pi\sigma\hat{\mathbf{n}}_{\rm surf}\ . \tag{4.1}$$

$\bar{E}_{\rm out}$ and $\bar{E}_{\rm in}$ are the electric fields in the plane perpendicular to the wire just outside and just inside the interface, and $\hat{\mathbf{n}}_{\rm surf}$ is the unit vector normal to the surface. Conversely, knowledge of $\sigma$ suffices to determine the field everywhere from

$$\Phi(\mathbf{r})=\int\frac{d\,\mathbf{A}\sigma(\mathbf{A})}{|\mathbf{r}-\mathbf{r}_{\mathbf{A}}|}\ , \tag{4.2}$$

where the integration is over the interface.

Consider a wire of infinite length and arbitrary cross section. Owing to symmetry along the wire, the surface charge density can be written in the form $\sigma(\mathbf{A})=\sigma(s)\exp(ikz)$ where $s$ parametrizes the position around the wire perimeter. The $z$ integration in Eq. (4.2) can be performed analytically, yielding

$$\phi(\bar{\rho})=2\oint ds\,\sigma(s)K_0(k|\bar{\rho}-\bar{\rho}_s|)\ , \tag{4.3}$$

where $\bar{\rho}_s$ is the vector position of a location on the wire perimeter parametrized by $s$. The gradient of Eq. (4.3) can be used to calculate the electric field everywhere except at the interface, where the bound surface charge induces discontinuities in the normal component of $\bar{E}$. Careful differentiation of Eq. (4.3) with respect to $\bar{\rho}$ yields the following formulas for the electric fields just inside and outside the wire:

$$\bar{E}_{\rm in}(s)=2k\oint ds'\sigma(s')\hat{\rho}_{ss'}K_1(k\rho_{ss'})-2\pi\sigma(s)\hat{\mathbf{n}}_s\ , \tag{4.4}$$

$$\bar{E}_{\rm out}(s)=2k\oint ds'\sigma(s')\hat{\rho}_{ss'}K_1(k\rho_{ss'})+2\pi\sigma(s)\hat{\mathbf{n}}_s\ , \tag{4.5}$$

where $\rho_{ss'}\equiv|\bar{\rho}_s-\bar{\rho}_{s'}|$, and $\hat{\rho}_{ss'}\equiv(\bar{\rho}_s-\bar{\rho}_{s'})/\rho_{ss'}$. It is easy to see that Eqs. (4.4) and (4.5) satisfy Eq. (4.1). By requiring continuity in the normal component of $\bar{D}$ we obtain the desired integral equation

$$\oint ds'\sigma(s')A(s,s')=\lambda\sigma(s)\ , \tag{4.6}$$

where $\lambda=[\epsilon_1(\omega)+\epsilon_2(\omega)]/[\epsilon_1(\omega)-\epsilon_2(\omega)]$ as before, and $A(s,s')=\pi^{-1}kK_1(k\rho_{ss'})\hat{\mathbf{n}}_s\cdot\hat{\rho}_{ss'}$.

A few points about Eq. (4.6) are worth mentioning. The diagonal elements of the kernel can be seen to satisfy the condition $A(s,s)=(2\pi C_s)^{-1}$ where $C_s$ equals the radius of curvature of the boundary at point $s$. The kernel is finite everywhere, so the spectrum of eigenvalues is discrete[21] and satisfies the sum rule $\sum_m\lambda_m=\oint ds\,A(s,s)=\oint ds\,(2\pi C_s)^{-1}=1$. Here the mode index $m$ approximately equals half the number of nodes of $\sigma_m(s)$ going around the wire circumference, so $m$ continues to play the role of an azimuthal quantum number. For the case $(k,m)\neq(k',m')$ we have been able to show that the interface modes are orthogonal in the sense that $\int d^3x\,\mathbf{E}_{km}(\mathbf{x})\cdot\mathbf{E}_{k'm'}(\mathbf{x})=0$. At $k=0$ the following physical argument shows that one of the eigenvalues equals unity. Consider the charge distribution $\sigma_0(s)$ which would occur if net charge were placed on a *conducting* wire of the same shape as the dielectric one considered here surrounded by vacuum. $\bar{E}_{\rm in}(s)$ vanishes for such a

charge distribution. To see that $\sigma_0(s)$ is an eigenfunction of Eq. (4.6) with eigenvalue $\lambda=1$, substitute $\sigma_0(s)$ into Eq. (4.4) and take the dot product of the resulting equation with $\hat{\mathbf{n}}_s$. This eigenvalue $\lambda=1$ corresponds to $\omega$ equaling either $\omega_{\mathrm{LO},2}$ or $\omega_{\mathrm{TO},1}$, which was seen to be the case for the $k=0, m=0$ mode of the elliptical and circular cross sections discussed in the previous section. The physical meaning of this mode will be discussed in Sec. VI.

A number of methods exist to solve Eq. (4.6) numerically. Most of them involve the diagonalization of a large matrix. We choose to do this by approximating the integral over $s$ by a sum over $N$ appropriately spaced points $s_i$ and solving the matrix eigenvalue problem

$$\sum_{j=1}^{N} A_{ij}\sigma_j=\lambda\sigma_i \ , \tag{4.7}$$

where $\sigma_i=\sigma(s_i)$ and $A_{ij}=(s_{j+1}-s_j)A(s_i,s_j)$. This simple approach is expected to yield reasonable results for eigenfunctions $\sigma(s)$ which vary slowly on the scale of $s_{j+1}-s_j$.

As an example of the present method, we consider a wire consisting of two flat parallel strips which are joined at the edges by two half cylinders. The cross section of this wire ("oval") is indicated by the short-dashed line in Fig. 1. This system has the same symmetry as an ellipse so that the solutions to Eq. (4.6) have the same symmetries as those described in Sec. III. The numerical results are found to converge well for $\sigma_m(s)$ when $N$ greatly exceeds $\max(kr,m)$. A plot of the eigenvalues $\lambda_m$ for the oval cross section is given in Fig. 5 as a function of $k$. The results are qualitatively similar to those for the ellipse, which was shown in Fig. 2. For instance, as either $k$ or $m$ becomes large, $\lambda_m(k)$ approaches zero, which is the result for a planar interface. Also, the eigenvalue of the $m=0$ mode $[\lambda_0(k)]$ equals unity at $k=0$, as previously noted. The potential generated by this mode is

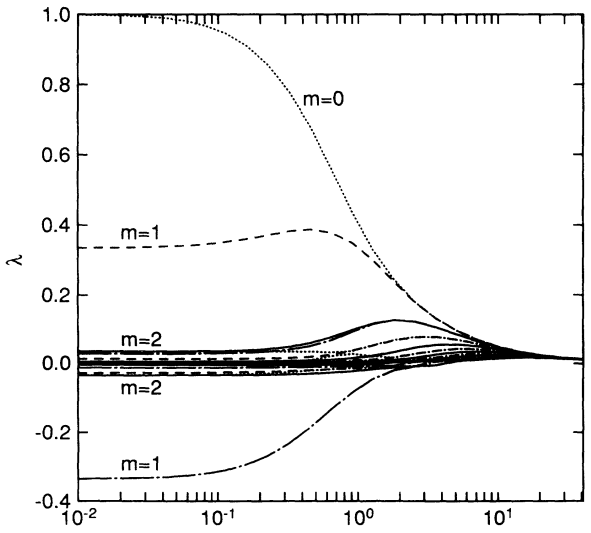


FIG. 5. Eigenvalues $\lambda_m(k)$ for the oval case (wire cross section indicated by short-dashed line in Fig. 1). The notation is the same as in Fig. 2.

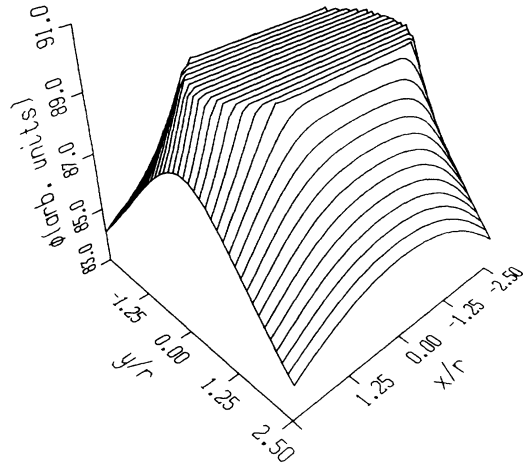


FIG. 6. The reduced potential $\phi(x,y)$ generated by the $m=0$ mode of the wire with oval cross section, the shape of which is indicated by the short-dashed line in Fig. 1. Here $kr$ equals zero.

shown in Fig. 6. Note that $\phi(x,y)$ is constant throughout the wire interior, so **E** is parallel to the wire in this region. An interesting difference between the results for the ellipse and those for the oval are the presence of "avoided crossings" in $\lambda_m(k)$ for the oval (although difficult to discern visually in Fig. 5). This results from the fact that Eq. (2.2) and the boundary conditions are not simultaneously separable for the latter geometry.

## V. RECTANGULAR WIRE

The interface modes of a wire with rectangular cross section cannot be solved analytically. Because of its sharp corners a rectangular cross section also poses a special difficulty for the numerical technique discussed in Sec. IV. The diagonal element of the kernel of Eq. (4.6) is inversely proportional to the local radius of curvature, so it diverges at the corners. In practical physical situations the wires often will be represented by continuum models having rounded corners with curvature radii $a$ on the order of an atomic radius, which avoids this mathematical problem. Here we study wires whose cross sections are rectangles with rounded corners having various values of corner radius $a$ as shown in Fig. 1.

As $a$ becomes significantly smaller than both $k^{-1}$ and the wire diameter, the numerical results approach a well-defined limit. We show in Appendix B that for the limiting case (rectangle) the spectrum of eigenvalues is, in fact, continuous in the range $-\frac{1}{2}<\lambda<\frac{1}{2}$ independent of $k$. For the general case of a wire with one (or more) sharp corner(s) the spectrum of Eq. (4.6) is continuous in the range $|\lambda|<|1-2\beta/\pi|$, where $2\beta$ is the angle ($=\pi/2$ for a rectangle) subtended by the particular corner that deviates the most from flatness. This result contrasts with the discrete spectra seen in Figs. 2 and 5 for the elliptical and oval cross sections, respectively. This is the most striking effect of the kernel's singular nature when the corners are infinitely sharp. Dispersion relations for rectangular wires with rounded corners are shown in Figs. 7(a) and 7(b) for values of $r/a$ equaling 10 and $10^5$, respectively

(corresponding to the solid and dotted lines, respectively, in Fig. 1). Figure 7(b) illustrates the approach to continuous spectrum described above for cross sections having sharp corners. Exactly one mode ($m=0$) is discretely separated from the continuum but approaches it rapidly as $kr \to \infty$. Its discrete separation from the continuum is guaranteed by the fact that $\lambda_0(k \to 0)=1$ as discussed earlier. For other wire cross sections having corners, other interface modes (i.e., $m \neq 0$) might also be discretely separated from the continuum for small and moderate $k$.

From an examination of the modes for $kr \gtrsim 1$ we find that those with eigenvalues near $\lambda=\pm\frac{1}{2}$ tend to be localized in the corners of wires having approximately rectangular cross sections. This is shown quite strikingly in Fig. 8 for an $m=0$ mode at $kr=2$. Localization of modes in the sharp portions of a wire with elliptical cross section was shown in Fig. 4. In general one expects that modes may be localized near "defects" like the corners of these wires. This has been seen for acoustic phonons near corners of elastic materials[25] and for short-wavelength surface phonons of stepped crystals.[26] A previous study[17] of interface phonons for a wire of rectangular cross section did not obtain a complete description of these corner modes.

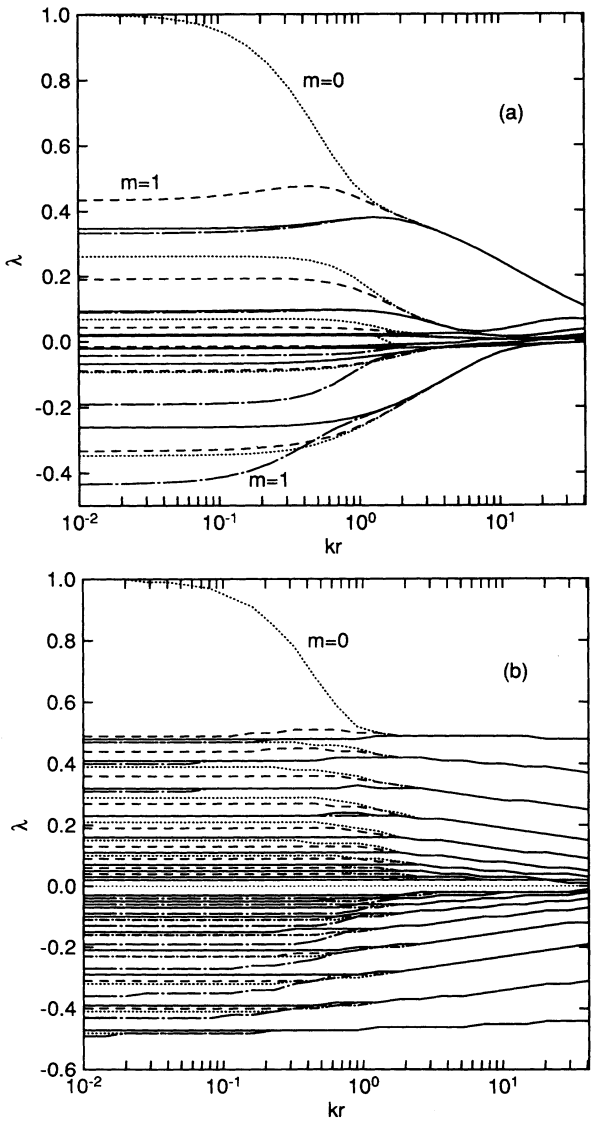


FIG. 7. Eigenvalues $\lambda_m(k)$ for the rectangular case having $R/r=2$ and (a) $r/a=10$ or (b) $r/a=10^5$. The wire cross section is indicated by the solid line or the dotted line, respectively, in Fig. 1. The quantities $(R,r,a)$ are defined in Fig. 1. The notation is the same as in Fig. 2.

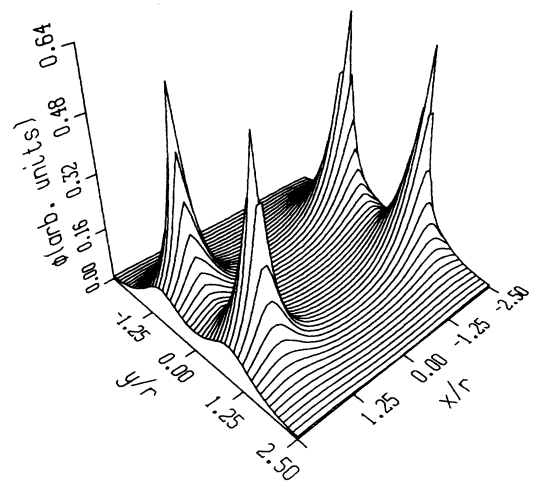


FIG. 8. The reduced potential $\phi(x,y)$ generated by the $m=0$ mode of a wire with rectangular cross section having $R/r=2$ and corner curvature $a=r/10$. Here $kr=2$.

Additional insight can be gained into the spatial behavior of these corner modes by noting that for modes in the vicinity of the corner, the local environment can be approximated by a single corner between two semi-infinite planes as shown in Fig. 9. Details of the properties of

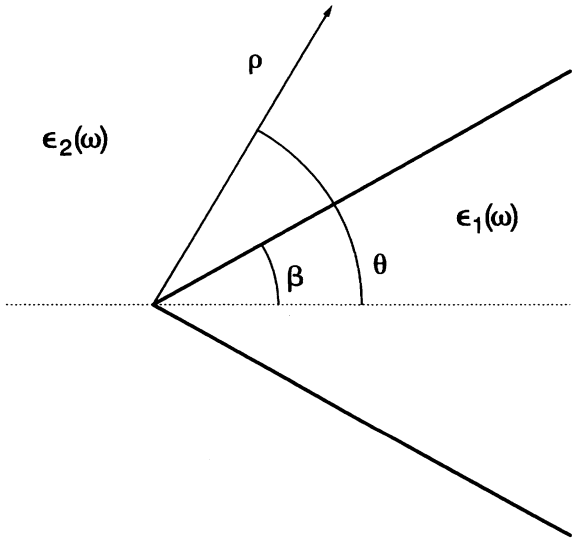


FIG. 9. Cross section of a single corner (as discussed in Appendix A) formed from two semi-infinite planes which separate two different dielectric materials.

this system are given in Appendix A. There it is shown that the localization length $L$ of the modes in the corners decreases with increasing $k$ and, in particular, that $L$ is on the order of $k^{-1}\max(1,(2/\pi)\mathrm{sech}^{-1}(2|\lambda|))$. For localized modes with $\lambda\sim+\frac{1}{2}$ the electrostatic potential generated is well approximated by a line of oscillating (i.e., $e^{ikz}$) charge density situated along the corner. For localized modes with $\lambda\sim-\frac{1}{2}$, the potential is approximately that due to a line of oscillating *dipole* density. Hence the sign of $\lambda_m$, or equivalently that of $\omega_{\mathrm{IF}}-\omega_m$, as well as its magnitude, dictates the qualitative spatial dependence of the potential generated by a particular interface phonon. This, in turn, should affect the strength of the electron-phonon coupling.

## VI. DISCUSSION

In the present work, we have used the continuum approach to study the optical-interface phonons of quantum wires with a number of different cross-sectional shapes. Analytical results have been obtained for wires having elliptical cross sections, and numerical results based on an integral-equation approach have been given for wires with other cross sections. One of the interesting features obtained in this work has been the appearance of modes localized in the corners of wire cross sections. The degree of localization has been found to increase with increasing sharpness of the corners. A recent lattice-dynamical study[12] of a particular quantum-wire array also has obtained corner modes.

A useful way to understand a number of the properties obtained here for the interface modes of quantum wires is to compare them with corresponding results for quantum wells, systems which have been subjected to considerably more study. The characteristics of quantum-well interface modes calculated from the continuum approach resemble closely those from more detailed calculations.[9,10,27,28] For the quantum well there are four interface modes. The two modes with frequencies between $\omega_{\mathrm{TO},1}$ and $\omega_{\mathrm{LO},1}$ (corresponding to the well material) are of particular interest here. At vanishingly small wave vector $\bar{k}$ parallel to the plane of the quantum well, one of these has eigenvalue $\lambda=-1$, frequency $\omega=\omega_{\mathrm{LO},1}$, and polarization perpendicular to the plane of the quantum well. The other has $\lambda=1$, frequency $\omega=\omega_{\mathrm{TO},1}$, and polarization parallel to the well. For the former mode the Coulomb field arising from the bound charge at the interfaces of the well causes vibrations to be at the bulk-LO phonon frequency, whereas the lack of such a field for the latter interface mode causes it to vibrate at the bulk-TO frequency. This reversal of the polarization-frequency relationship for LO and TO modes in a quantum well as compared to the bulk has been noted previously.[9,28] At larger wave vectors $\bar{k}$ the quantum-well interface modes become increasingly localized on the two interfaces, and their frequencies approach that of the isolated interface.

In the case of the wire geometry for vanishingly small wave vector along the wire, there is only one longitudinally polarized interface mode. This is the $m=0$ mode, which has eigenvalue $\lambda=1$ and frequency $\omega=\omega_{\mathrm{TO},1}$, as does the interface mode with corresponding polarization in the quantum well. There is no modification of its frequency due to the wire confinement, and thus it is a feature common to all wire cross sections. In the case of the quantum well there has been discussion in the literature concerning the construction of a complete set of phonon states from the interface and confined bulk modes derived by a continuum approach.[9,10,27] For the quantum wire we have seen that at small wave vector the potential generated by the $m=0$ mode fills the wire uniformly and looks like a nodeless bulk mode as seen, for example, in Fig. 6. We suggest that this mode be best thought of as an interface mode and that no corresponding mode should be included among the bulk confined modes in constructing a complete set of states for the wire.

In the wire geometry there are two polarizations perpendicular to the wave vector. The frequencies of these modes are influenced by the Coulomb interactions from the sides of the wire, which depend on shape. At long wavelengths no mode occurs with eigenvalue $\lambda=-1$ ($\omega=\omega_{\mathrm{LO},1}$), because of modifications to the long-range interactions as compared to the case of the quantum well. For increasing $m$ the modes are more localized in the interface region, and thus their frequencies approach $\omega=\omega_{\mathrm{IF}}$, that of the planar interface. For a given $m$ the two modes have different symmetries, and different Coulomb interactions for the two modes gives rise to a splitting between them. The case of $k=0$, $m\neq0$ modes of the ellipse shown in Fig. 2 provides a useful illustration. Pairs of these modes with equal values of $m$ have equal and opposite values of $\lambda$. The upper modes are symmetric about the $x$ axis, whereas the lower modes are antisymmetric about the $x$ axis. In this regard the case of the circular cross section is an interesting limit. For this limit, each of the modes for a given $m$ are equivalent by symmetry; therefore, their eigenvalues $\lambda$ are degenerate and must equal zero (corresponding to $\omega=\omega_{\mathrm{IF}}$).

The continuum approach provides a simple, clear picture of the interface phonon modes of confined structures. This approach has been used extensively to obtain analytic results for electron-phonon coupling in quantum wells where scattering from interface modes has been found to be particularly important. In this regard the present results should prove useful for studying electron-phonon scattering in quantum-wire systems. The continuum approach also provides a model within which there is clear distinction between interface and bulk confined modes. In the present work we have made a comprehensive study of the properties of interface phonons of quantum wires using this approach. We have explored the systematic variations of the features of the interface phonons with the shape of the wire cross section and have related them to corresponding results for quantum wells.

Certain limitations of a continuum model might be noted. For instance, to apply a continuum theory to a quantum well the number of atomic layers must be large, and the wave vector must be less than the Debye wave vector $k_D=O(a^{-1})$ where $a$ is the lattice constant. This also holds true for a wire, and in addition the mode index $m$ must be less than $O(r/a)$ for a wire of radius $r$. Also, a realistic wire with rectangular cross section should have

corners rounded on the scale of at least one lattice constant, which would eliminate the unphysical behavior associated with sharp corners discussed in Sec. V and Appendixes A and B. The dispersion of the bulk-LO and -TO phonons will give rise to some mixing of the interface and bulk confined modes. The present continuum approach does not include this dispersion, and thus it does not give a description of this coupling. This issue is studied better using a lattice-dynamics approach for particular systems such as those done in two recent studies.[12,13]

The methods used here may be useful for the study of interface phonons of other confined systems. For example quantum dots of various shapes and systems composed of either line defects or several wires can, depending on the specific geometry, be treated either analytically or by generalizations of the integral equation approach used here. In addition, other excitations such as interface plasmons can be treated with a dielectric formalism similar to the one used here.


## ACKNOWLEDGMENTS

One of us (P.A.K.) was supported by the National Research Council and also acknowledges helpful conversations with F. Robicheaux during this work. One of us (T.L.R.) acknowledges the support of the Office of Naval Research and has benefited from conversations with S. Rudin. We thank G. Brozak, D. G. Gammon, and B. V. Shanabrook for critical readings of this manuscript.


## APPENDIX A: BEHAVIOR NEAR A CORNER

Near a sharp corner in a wire cross section the environment is approximated by a single corner separating two semi-infinite planes which, in turn, separate two different dielectric media as shown in Fig. 9. The angle $2\beta$ between the two planes equals $\pi/2$ for a wire with rectangular cross section, but for reasons of generality we allow it to take any value in the range $0<2\beta<2\pi$. Here we study the properties of such an isolated corner, for which Eq. (2.2) and the boundary conditions separate in cylindrical coordinates $(\rho,\theta)$. Taking $\phi(\rho,\theta)\equiv T(\theta)R(\rho)$, the one-dimensional differential equations are

$$\frac{d^2T}{d\theta^2}-\gamma^2=0$$

and (A1)

$$\frac{\rho^2 d^2R}{d\rho^2}+\frac{\rho\, dR}{d\rho}+(\gamma^2-k^2\rho^2)R=0\ ,$$

where $\gamma^2$ is the separation constant. The boundary conditions that $\lim_{\rho\to\infty}R(\rho)$ and $\lim_{\rho\to 0}R(\rho)$ are both finite restrict $\gamma^2$ to being real and positive.[29] For definiteness we take $\gamma>0$. The radial solutions are Bessel functions of imaginary index (given by $i\gamma$) and of imaginary argument (given by $ik\rho$). When $\rho\gg\gamma/k$, then $R(\rho)\sim\exp(-k\rho)$, and when $\rho\ll\gamma/k$, then $R(\rho)=\cos(\gamma\ln\rho+\delta)$. Hence the quantity $L=k^{-1}\max(1,\gamma)$ defines a localization length beyond which $\phi$ decays exponentially. The quantity $\gamma$ represents the rapidity of oscillations as $\rho\to 0$ and so is analogous to the mode index $m$. Note that $R(\rho)$ has an infinite number of oscillations as $\rho\to 0$. It might be noted that this unphysical behavior is eliminated either if the corner is slightly rounded or if $\epsilon(\omega)$ has a $q$ dependence.

The angular solutions can be chosen to be either even or odd with respect to reflection through the $\theta=0$ plane:

$$T_+(\theta)=\begin{cases}\cosh\gamma(\pi-\beta)\cosh\gamma\theta, & |\theta|\le\beta\\ \cosh\gamma(\pi-\theta)\cosh\gamma\beta, & \pi\ge|\theta|\ge\beta\ ,\end{cases}\tag{A2}$$

$$T_-(\theta)=\begin{cases}\sinh\gamma(\pi-\beta)\sinh\gamma\theta, & |\theta|\le\beta\\ \sinh\gamma(\pi-\theta)\sinh\gamma\beta, & \pi\ge|\theta|\ge\beta\ ,\end{cases}\tag{A3}$$

where $2\beta$ is the angle formed by the two planes (Fig. 9). Here the $\pm$ subscript indicates the parity of $T(\theta)$ with respect to reflection through the $\theta=0$ plane. By requiring that the normal component of $\bar{D}$ be continuous we obtain

$$\lambda_\pm=\frac{\epsilon_1(\omega)+\epsilon_2(\omega)}{\epsilon_1(\omega)-\epsilon_2(\omega)}=\pm\frac{\sinh\gamma(\pi-2\beta)}{\sinh\gamma\pi}\ .\tag{A4}$$

As $\gamma$ ranges from $\infty$ to 0 the quantity $\lambda_+$ ($\lambda_-$) ranges continuously and monotonically from 0 to $1-2\beta/\pi$ (to $2\beta/\pi-1$), which leads to a continuous spectrum as noted in the text. A more rigorous proof of this fact is given in Appendix B.

The limiting case $\gamma=0$ deserves special attention. The radial solutions are $R_\pm^{(0)}(\rho)=K_0(k\rho)$, and the angular solutions are

$$T_+^{(0)}(\theta)=\text{const}$$

and (A5)

$$T_-^{(0)}(\theta)=\begin{cases}(\pi-\beta)\theta, & |\theta|\le\beta\\ (\pi-\theta)\beta, & \pi\ge|\theta|\ge\beta\ .\end{cases}$$

Straightforward application of boundary conditions yields $\lambda_-^{(0)}=2\beta/\pi-1$. However, the result that $\lambda_+^{(0)}=1-2\beta/\pi$ is obtained by encircling the edge with an imaginary cylindrical surface and applying Gauss's law. The charge density corresponding to the even-parity solution is nonzero only at $\rho=0$, so it might be called a corner mode. The relative atomic displacements for these (and other) interface phonons are simply proportional to the polarization $\mathbf{P}=(\epsilon-\epsilon_\infty)\mathbf{E}/4\pi$. Sufficiently near the corner ($\rho\ll k^{-1}$) the polarizations for the symmetric and antisymmetric corner modes, respectively, are $\mathbf{P}_+\sim e^{ikz}\rho^{-1}\hat{\rho}$ and $\mathbf{P}_-\sim e^{ikz}\rho^{-1}\hat{\theta}\ln k\rho$. Hence, near the corner the polarizations of both the symmetric and antisymmetric corner modes diverge and are perpendicular to both $\mathbf{k}(=k\hat{\mathbf{z}})$ and each other. In fact, the surface charge density for the $\gamma\neq 0$ modes is proportional to $R_\pm(\rho)/\rho$, so *all* of the interface modes (and fields generated by them) are partially localized to within a particular distance [$\sim k^{-1}\max(1,\gamma)$] of the corner. For a rectangular corner ($2\beta=\pi/2$), Eq. (A4) can be inverted to yield

$$\gamma=\frac{2}{\pi}\ln\frac{1+\sqrt{1-4\lambda^2}}{2|\lambda|}\ .\tag{A6}$$

Hence the corner localization length in this case is given by

$$L(k,\lambda)=k^{-1}\max\left[1,\frac{2}{\pi}\ln\frac{1+\sqrt{1-4\lambda^2}}{2|\lambda|}\right]. \quad \text{(A7)}$$

## APPENDIX B: CONTINUOUS SPECTRUM FOR A WIRE WITH A SHARP CORNER

In order to show that the spectrum of Eq. (4.6) is continuous in the range $|\lambda|<|1-2\beta/\pi|$ for a wire cross having a sharp corner of angle $2\beta$, it suffices to show that

$$\lim_{n\to\infty}\frac{\left|\left|\oint ds' A(s,s')f_n(s')-\lambda f_n(s)\right|\right|}{\|f_n(s)\|}=0 , \quad \text{(B1)}$$

where $\{f_n(s)\}$ is an infinite sequence of functions [not necessarily solutions of Eq. (4.6)] and $\|f(s)\|\equiv\int ds|f(s)|$ (see, e.g., Sec. 5.6 of Ref. 24). We choose $f_n(s)$ as

$$f_n(s)=\tau_\lambda(s)\times\begin{cases}\dfrac{\cos(\gamma\ln\rho_{s0})}{\rho_{s0}}, & \rho_{s0}\geq r_n>0\\ 0 \text{ otherwise} .\end{cases} \quad \text{(B2)}$$

Here $s'=0$ defines the position of a particular corner, $\lim_{n\to\infty}r_n=0$, and $\gamma(>0)$ is related to $\lambda$ by $|\lambda|=(\sinh\gamma\pi|1-2\beta/\pi|)/\sinh\gamma\pi$. Also $\tau_\lambda(s)=1$ if $\lambda$ is positive, but takes on the following functional form if $\lambda$ is negative:

$$\tau_{\lambda<0}(s)=\begin{cases}1, & s>0,\ \rho_{s0}<r_0\\ -1, & s<0,\ \rho_{s0}<r_0\\ O(1) \text{ otherwise} .\end{cases} \quad \text{(B3)}$$

For later convenience we define $r_0$ to be much smaller than both $k^{-1}$ and any (nonzero) radius of curvature $C_s$ along the wire. The following proof takes advantage of the fact (shown in Appendix A) that if $\sigma_\lambda(s)$ is a solution of Eq. (4.6) with eigenvalue $\lambda$ less than $|1-2\beta/\pi|$ in absolute value, then sufficiently near a corner $\sigma_\lambda(s)\sim\rho_{s0}^{-1}\cos(\gamma\ln\rho_{s0})$.

In order to prove Eq. (B1), first notice that

$$\lim_{n\to\infty}\|f_n(s)\|=O(\ln r_n^{-1})\to\infty .$$

Now we simply need to show that the numerator of Eq. (B1) is bounded. ($c_n$ is "bounded" if and only if $\lim_{n\to\infty}c_n<\infty$.) To do this we separate the range of integration (over $s$) into three disjoint regions: (1) $\rho_{s0}\geq r_0$, (2) $r_0\geq\rho_{s0}\geq r_n$, and (3) $r_n\geq\rho_{s0}$. Now $\|\cdots\|\equiv\|\cdots\|_1+\|\cdots\|_2+\|\cdots\|_3$. We will show that each of these is bounded, in turn.

*Region 1.* $\lambda f_n(s)$ is obviously bounded. To see that $\int ds' A(s,s')f_n(s')$ is bounded, first realize that

$$\oint_{\rho_{s'0}\geq r_0}ds' A(s,s')f_n(s')=\oint_{\rho_{s'0}\geq r_0}ds' A(s,s')f_0(s')$$

is bounded, because neither $A(s,s')$ nor $f_0(s')$ is singular in this region. Next, note that

$$\oint ds' A(s,s')f_n(s')\sim[A(s,\epsilon)\pm A(s,-\epsilon)]\int_0^{\rho_{s'0}=r_0}ds' f_n(s')$$
$$\sim[A(s,\epsilon)\pm A(s,-\epsilon)][\sin(\gamma\ln r_0)-\sin(\gamma\ln r_n)]/\gamma ,$$

which is bounded. (In these and future equations the top sign is taken if $\lambda>0$ and the bottom one is taken if $\lambda<0$.) Hence

$$\left|\left|\oint ds' A(s,s')f_n(s')-\lambda f_n(s)\right|\right|_1$$

is bounded.

*Region 2.*

$$\oint ds' A(s,s')f_n(s')\sim\pm k\sin2\beta\int_0^\infty\rho\,d\rho\,f_n(\rho)\frac{K_1(k\sqrt{\rho^2+\rho_{s0}^2-2\rho\rho_{s0}\cos2\beta})}{\pi\sqrt{\rho^2+\rho_{s0}^2-2\rho\rho_{s0}\cos2\beta}}$$

(because $r_0\ll C_s$)

$$\sim\pm\frac{\sin2\beta}{\pi}\int_0^\infty\rho\,d\rho\,f_n(\rho)/(\rho^2+\rho_{s0}^2-2\rho\rho_{s0}\cos2\beta)$$

(because $r_0\ll k^{-1}$)

$$=\pm\frac{\sin2\beta}{\pi}\int_{r_n}^\infty d\rho(\rho^2+\rho_{s0}^2-2\rho\rho_{s0}\cos2\beta)^{-1}\cos(\gamma\ln\rho) .$$

Also,

$$\lambda f_n(s)=\pm\frac{\sinh\gamma(\pi-2\beta)\cos(\gamma\ln\rho_{s0})}{(\sinh\gamma\pi)\rho_{s0}}=\pm\frac{\sin2\beta}{\pi}\int_0^\infty d\rho(\rho^2+\rho_{s0}^2-2\rho\rho_{s0}\cos2\beta)^{-1}\cos(\gamma\ln\rho)$$

(see Sec. 3.983 of Ref. 23). Hence,

$$\left|\oint ds' A(s,s')f_n(s')-\lambda f_n(s)\right| = \left|\frac{\sin 2\beta}{\pi}\int_0^{r_0} d\rho(\rho^2+\rho_{s0}^2-2\rho\rho_{s0}\cos 2\beta)^{-1}\cos(\gamma\ln\rho)\right|$$
$$\leq \pi^{-1}\int_0^{r_0} d\rho(\rho^2+\rho_{s0}^2-2\rho\rho_{s0}\cos 2\beta)^{-1}$$
$$\leq \pi^{-1}\int_0^{r_0} d\rho(\rho_{s0}-\rho\cos 2\beta)^{-2}$$
$$= r_n/[\pi\rho_{s0}(\rho_{s0}-\rho_n\cos 2\beta)] \leq \frac{r_n}{\rho_{s0}^2(1-\cos 2\beta)} ,$$

so

$$\left|\left|\oint ds' A(s,s')f_n(s')-\lambda f_n(s)\right|\right|_2 \leq O\left[\int_{r_n}^{\infty} r_n d\rho/\rho^2\right] = O(1) ,$$

which is bounded.

*Region 3.* First note that $\lambda f_n(s)=0$. Next,

$$\left|\oint ds' A(s,s')f_n(s')\right| \sim \left|\frac{\sin 2\beta}{\pi}\int_{r_n}^{\infty} d\rho(\rho^2+\rho_{s0}^2-2\rho\rho_{s0}\cos 2\beta)^{-1}\cos(\gamma\ln\rho)\right|$$
$$\leq \pi^{-1}\int_{r_n}^{\infty} d\rho/(\rho-\rho_{s0}\cos 2\beta)^2 = [\pi(r_n-\rho_{s0}\cos 2\beta)]^{-1} \leq [\pi r_n(1-\cos 2\beta)]^{-1} ,$$

so

$$\left|\left|\oint ds' A(s,s')f_n(s')-\lambda f_n(s)\right|\right|_3 \leq O(r_n/r_n) = O(1) ,$$

which is bounded. Hence,

$$\left|\left|\oint ds' A(s,s')f_n(s')-\lambda f_n(s)\right|\right| \Big/ \|f_n(s)\| \leq [O(1)+O(1)+O(1)]/O(\ln r_n^{-1}) = O(-1/\ln r_n) \to 0 ,$$

so the spectrum of Eq. (4.6) is continuous is the range $|\lambda| < |1-2\beta/\pi|$.


[1] M. Tsuchiya, J. M. Gaines, R. H. Yan, R. J. Simes, P. O. Holtz, L. A. Coldren, and P. M. Petroff, Phys. Rev. Lett. **62**, 466 (1989).

[2] M. V. Klein, IEEE J. Quantum Electron. **QE-22**, 1760 (1986); M. Cardona, in *Lectures on Surface Science,* edited by G. R. Castro and M. Cardona (Springer-Verlag, Berlin, 1987), pp. 2–27, and references therein.

[3] A. K. Sood, J. Menéndez, M. Cardona, and K. Ploog, Phys. Rev. Lett. **54**, 2111 (1985).

[4] Ronald Fuchs and K. L. Kliewer, Phys. Rev. **140**, A2076 (1965).

[5] James J. Licari and Roger Evrard, Phys. Rev. B **15**, 2254 (1977).

[6] See, for example, *Surface Excitations,* edited by V. M. Agranovich and R. Loudon (North-Holland, Amsterdam, 1984).

[7] S. Rudin and T. L. Reinecke, Phys. Rev. B **41**, 7713 (1990); B. K. Ridley, *ibid.* **39**, 5282 (1989).

[8] Ph. Lambin, P. Senet, and A. A. Lucas, Phys. Rev. B **44**, 6416 (1991).

[9] Kun Huang and Bang-Fen Zhu, Phys. Rev. B **38**, 2183 (1988).

[10] H. Rücker, E. Molinari, and P. Lugli, Phys. Rev. B **44**, 3463 (1991).

[11] M. Watt, C. M. Sotomayor Torres, H. E. G. Arnot, and S. P. Beaumont, Semicond. Sci. Techol. **5**, 285 (1990).

[12] Shang-Fen Ren and Yia-Chung Chang, Phys. Rev. B **43**, 11 857 (1991).

[13] Bang-fen Zhu, Phys. Rev. B **44**, 1926 (1991).

[14] N. C. Constantinou and B. K. Ridley, Phys. Rev. B **41**, 10 622 (1990); **41**, 10 627 (1990).

[15] R. Ruppin and R. Englman, Rep. Prog. Phys. **33**, 149 (1970).

[16] Michael A. Stroscio, Phys. Rev. B **40**, 6428 (1989).

[17] Michael A. Stroscio, K. W. Kim, Michael A. Littlejohn, and Hsuhung Chuang, Phys. Rev. B **42**, 1488 (1990); Michael A. Stroscio, K. W. Kim, and M. A. Littlejohn, Proc. SPIE **1362**, 566 (1990); M. A. Stroscio, K. W. Kim, and Amit Bhatt, Bull. Am. Phys. Soc. **36**, 825 (1991).

[18] The relative merits of electrostatic or mechanical boundary conditions, which has been discussed for bulk confined modes (Refs. 2, 9, and 10), does not arise in the case of interface modes.

[19] Other interface modes, e.g., interface plasmons, can be studied by taking appropriate forms of the dielectric function $\epsilon(\omega)$.

[20] K. L. Kliewer and Ronald Fuchs, Phys. Rev. **144**, 495 (1966); P. A. Knipp and T. L. Reinecke (unpublished).

[21] Philip M. Morse and Herman Feshbach, *Methods of Theoretica Physics* (McGraw-Hill, New York, 1953).

[22] N. W. McLachlan, *Theory and Application of Mathieu Functions* (Clarendon, Oxford, 1947).

[23]I. S. Gradshteyn and I. M. Ryzhik, *Table of Integrals, Series, and Products* (Academic, New York, 1980).
[24]Ivar Stakgold, *Green's Functions and Boundary Value Problems* (Wiley, New York, 1979).
[25]A. A. Maradudin, R. F. Wallis, D. L. Mills, and R. L. Ballard, Phys. Rev. B **6**, 1106 (1972).
[26]P. Knipp, Phys. Rev. B **43**, 6908 (1991).
[27]R. Enderlein, Phys. Rev. B **43**, 14 513 (1991).
[28]R. Lassnig, Phys. Rev. B **30**, 7132 (1984).
[29]For a finite number of special interface modes, however, $\gamma^2$ can assume other values. These exceptional modes are characterized by the fact that their eigenvalue $\lambda$ does not fall within the continuum discussed in Appendix B. An example is the $m=0$ mode of the rectangle, for which $\gamma^2=-\frac{4}{9}$ at $k=0$, as discussed in Sec. 2.11 of J. D. Jackson, *Classical Electrodynamics* (Wiley, New York, 1975).